

Theoretical and Spectroscopic Study of the Effect of Ring Substitution on the Adsorption of Anisole on Platinum

Norberto Bonalumi, Angelo Vargas, Davide Ferri, and Alfons Baiker*

Department of Chemistry and Applied Biosciences - ETH Zurich, CH - 8093 Zurich, Switzerland

Received: February 13, 2006; In Final Form: March 28, 2006

The adsorption of anisole, 3,5-dimethylanisole, and 3,5-bis-(trifluoromethyl)-anisole on Pt(111) was studied theoretically and compared to the adsorption of benzene using relativistically corrected density functional theory. A cluster of 31 platinum atoms was used to simulate the surface. The three anisoles were found to be less strongly adsorbed than the parent molecule benzene, 3,5-bis-(trifluoromethyl)-anisole showing weakest adsorption, with an adsorption energy of only one-third that of benzene. The theoretical study was complemented by in situ ATR-IR spectroscopy of the adsorption of the anisole derivatives on a polycrystalline Pt film. The spectroscopic study indicated that the adsorption strength of the anisoles follows the same order as predicted by the calculations. In addition, catalytic hydrogenation tests showed that the propensity to aromatic ring hydrogenation can also be correlated to the mode and strength of adsorption of the anisoles. The degree of saturation followed the same order as the adsorption strength found by the calculations and indicated by spectroscopy. Although 3,5-dimethyl substitution on anisole resulted in only a partial loss of adsorption energy and reactivity toward ring hydrogenation as compared to anisole, the substitution by CF₃ groups led to a large loss of adsorption energy and complete loss of reactivity toward aromatic ring saturation. Along with the study of the substituent effect on the adsorption of aromatic molecules, the correlation between adsorption and propensity to saturation of aromatic substrates could be corroborated.

Introduction

The interaction of aromatic hydrocarbons with transition-metal catalysts is of considerable importance in various petrochemical processes. The adsorption of benzene on Pt single-crystal surfaces has been investigated in great detail using a number of UHV techniques, including RAIRS,¹ EELS² and HREELS,³ ARUPS,⁴ NEXAFS,⁵ diffuse LEED,⁶ and scanning tunneling microscopy.^{7,8} Only recently, it has been possible to locate the most stable adsorption sites of benzene on platinum with the help of density functional theory (DFT) studies of adsorption geometries and vibrational spectra.

Studies with both periodic boundary conditions (PBC) and metal cluster calculations^{9,10} agree that the most stable adsorption modes are on bridge and hollow sites (Figure 1) and that the former has higher adsorption energy than the latter. Experimental and theoretical data revealed that adsorption is coverage-dependent, benzene preferentially adsorbing at the bridge sites at low surface coverage.⁹ At complete coverage, a factor of 1.3 more molecules can be accommodated on hollow sites than on bridge sites, and because this value is larger than the ratio between the energy per surface atom of bridge and hollow sites, the latter are favored for high surface concentration. In this estimation, lateral repulsive interactions that destabilize the adsorbates have been neglected. For ethene adsorption these interactions have been estimated to about 2.1 kcal/mol per ethene–ethene interaction.¹¹ Note that when benzene is on a bridge site it forms σ -bonds with four surface atoms, whereas the binding is limited to three platinum atoms on hollow sites. It is useful to quantify the adsorption energy per surface atom using the experimental values of adsorption energies for

benzene, which are 29.0 and 20.1 kcal/mol for bridge and hollow sites, respectively (averages of 28.0–30.1 and 19.6–20.6 kcal/mol).¹² Moreover, the adsorption energy of benzene is 7.2 and 6.7 kcal/mol per surface atom for bridge and hollow sites, respectively.

The main results of the experimental studies of benzene adsorption on platinum are briefly summarized here: (i) the C₆ ring of benzene lies parallel to the metal surface but with some molecular distortion with respect to the gas-phase benzene induced by metal–adsorbate interactions, which results in the elongation of the C–C bonds; (ii) further distortion is obtained along the *z* axis perpendicular to the surface upon adsorption, which is induced by the rehybridization of carbon sp² electrons and formation of C–Pt σ bonds. As a consequence of the mentioned distortions, benzene exhibits a boat-like conformation on Pt where the hydrogen atoms point away from the molecular plane and from the surface; (iii) adsorption is typically disordered on most transition-metal surfaces at ambient temperature, some degree of ordering being given upon coadsorption of CO owing to adsorbate–adsorbate and electron donor–acceptor interactions.¹³

Little is still known on the effect that substituents have on the orientation of the C₆ ring with respect to a platinum surface and hence on the adsorption geometry of substituted benzenes. Studies on the adsorption of some monosubstituted benzenes over noble metals indicate that their surface chemistry is richer than that of the precursor due to the different reactivity of the aromatic ring, and to the possible presence of adsorbed species other than η^6 (“flat”).^{2,14–16} Detailed theoretical and vibrational studies on the adsorption behavior of some of the most common derivatives of benzene on platinum and on other transition metals are not yet available.

* To whom correspondence should be addressed. Phone: +41 44 632 31 53. Fax: +41 44 632 11 63. E-mail: baiker@chem.ethz.ch.

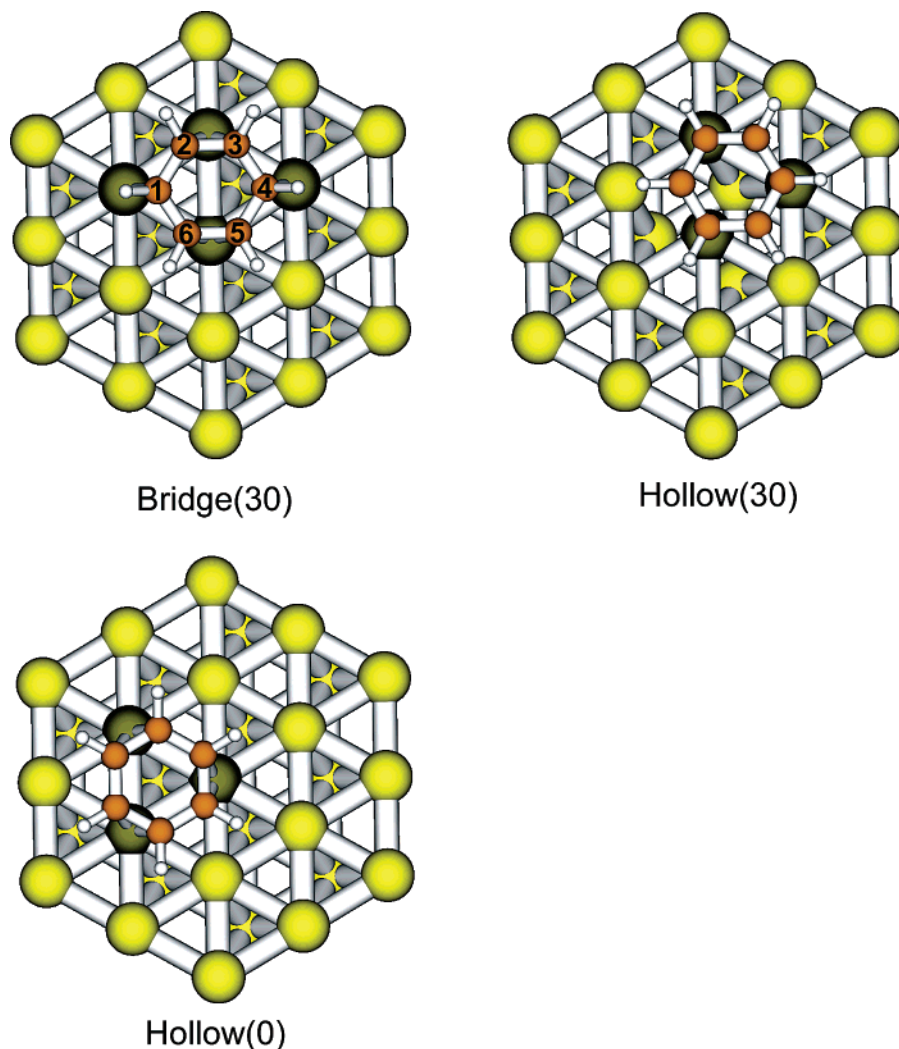
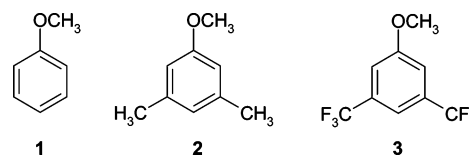


Figure 1. (a) Bridge(30), (b) hollow(30), and (c) hollow(0) adsorption of benzene on a Pt 31 cluster. Bridge adsorption of benzene: carbon atoms 1 and 4 are apical, and interact with only one platinum atom of the surface, while carbon atoms 2,3 and 5,6 are nonapical, and each couple interacts with only one platinum surface atom. The rehybridization of the aromatic carbon atoms changes for the apical and nonapical positions. The surface atoms to which benzene is bound are darkened.

Adsorption of aromatic hydrocarbons on Pt-based catalysts is also relevant to the production of fine chemicals and in particular to heterogeneous liquid-phase enantioselective hydrogenations, where activated ketones are reduced with high selectivity only to one of the possible enantiomers upon modification of the metal surface with a chiral agent.¹⁷ In this specific reaction, the optimum chiral modifier is a cinchona alkaloid, which has an aromatic moiety (quinoline) serving for the docking of the molecule to the metal surface. The quinoline moiety is partly responsible for the assorted adsorption chemistry demonstrated by the modifier on Pt.^{10,18,19} Adsorption of cinchonidine on Pt has been reported using spectroscopic techniques²⁰ and has been modeled by theoretical calculations.^{10,18,21} Investigation with vibrational spectroscopy techniques of the adsorption of cinchonidine and of complex synthetic cinchona alkaloids is simplified to some extent by the study of the behavior of the separate parts that constitute the relatively complex alkaloid, as demonstrated already in previous studies.^{16,20}

An important feature of enantioselective heterogeneous hydrogenations is that adsorption and reaction take place from solution and at the solid–liquid interface, respectively, so it is preferable to explore the behavior of the chiral modifier on a metal surface *in situ*, that is, in the presence of the solvent, rather than under UHV conditions. Reflection infrared tech-

SCHEME 1: Molecular Structure of Anisole (1) and Its Derivatives 3,5-Dimethylanisole (2) and 3,5-Bis-(trifluoromethyl)-anisole (3)



niques allow monitoring processes occurring in the liquid-phase to be in contact with solid surfaces with high sensitivity for surface species.²² The internal reflection mode²³ is best suited to compensate for most of the signal due to the solvent and is therefore the tool of choice for the spectroscopic studies of solid–liquid interfaces involving a strongly infrared-absorbing medium like a metal surface.

Recently, we have reported a combined spectroscopic and theoretical investigation of anisole (**1**, Scheme 1) on platinum, which served as an adsorption model for the determination of the local geometry of the alkaloid *O*-phenyl-cinchonidine on the metal surface.¹⁶ Because even more complex derivatives of *O*-phenyl-cinchonidine revealed interesting chiral modifiers in the enantioselective hydrogenation of activated ketones, the investigation of 3,5-dimethylanisole (**2**) and 3,5-bis-(trifluoro-

methyl)-anisole (**3**) adsorption on Pt appears crucial to understanding the behavior of aromatic ether derivatives of *O*-phenyl-cinchonidine. It also offers the opportunity to face under a broader perspective the question of how the substitution on the benzene ring can affect the adsorption properties of the ring in terms of adsorption energy and site.

With this in mind we investigated the adsorption behavior of the dimethyl- and bis-trifluoromethyl-derivatives of anisole and compared it to that of anisole and benzene using a combined approach including density functional theory (DFT) calculations and in situ attenuated total reflection infrared (ATR-IR) spectroscopy.

Experimental Section

Materials. Anisole (**1**, Scheme 1, Fluka, 99%), 3,5-dimethylanisole (**2**, Aldrich, >99%), and 3,5-bis-(trifluoromethyl)-anisole (**3**, ABCR) were used as received. Dichloromethane solvent (Baker, technical grade) was stored over 5 Å molecular sieve. N₂ (99.995 vol %) and H₂ (99.999 vol %) gases were supplied by PANGAS.

ATR-IR Spectroscopy. The Pt/Al₂O₃ thin films used for ATR-IR spectroscopy were prepared on a 1-mm-thick trapezoidal Ge internal reflection element (IRE, 50 × 20 × 2 mm³) by electron beam vapor deposition as described in detail elsewhere.²⁴ First, 50 nm Al₂O₃ was deposited followed by 1 nm Pt. A film was freshly prepared before each infrared measurement. In situ ATR-IR spectra were recorded on a Bruker Optics IFS-66/S spectrometer equipped with a commercial ATR accessory (Optispec) and a liquid-nitrogen-cooled MCT detector. Spectra were collected by co-adding 300 scans at 4 cm⁻¹ resolution. After fixing the freshly coated IRE within the cell walls and optics alignment the probe chamber was purged overnight. The homemade stainless steel flow-through cell was maintained at 20 °C throughout the experiments by a thermostat. N₂-saturated dichloromethane was circulated for about 30 min over the thin film at ca. 1.0 mL/min flow rate by a peristaltic pump to reach steady-state conditions. Before adsorption, the Pt film was contacted with H₂-saturated solvent for about 5 min. This procedure cleans the surface affording large domains of reduced Pt.²⁴ Then an H₂-saturated solution of the molecule under investigation (5 mM) was circulated through the cell for about 60 min followed by rinsing with H₂-saturated solvent in order to remove weakly adsorbed and dissolved species. ATR spectra are presented in absorbance units, and, where needed, signals from the gas-phase spectrum of water in the 1700–1400 cm⁻¹ spectral range were subtracted.

Theoretical Calculations. Adsorption studies have been performed using the Amsterdam Density Functional (ADF) program package.²⁵ The surface was simulated using a Pt 31 cluster for which the spin state was optimized ($\alpha - \beta = 8$). A frozen core approximation was used for the description of the inner core of the atoms. The orbitals up to 1s were kept frozen for the second row elements, whereas orbitals up to 4f were kept frozen for platinum. Decreasing the Pt frozen core to 4d, which implies the explicit calculation of 14 additional electrons per platinum atom, has been shown to increase the adsorption energy by only about 5 kJ/mol for the adsorption of benzene.⁹ The importance of relativistic effects has been shown for calculations involving platinum;^{26,27} therefore, the core was modeled using a relativistically corrected core potential created with the DIRAC utility of the ADF program. The DIRAC calculations imply the local density functional in its simple X- α approximation without any gradient correction, but the fully relativistic Hamiltonian is used, including spin-orbit coupling.

Furthermore, the relativistic scalar approximation (mass-velocity and Darwin corrections) was used for the Hamiltonian, with the zero order regular approximation (ZORA) formalism,²⁸ where spin-orbit coupling is included already in zero order. The first-order Pauli formalism²⁹ was shown to have theoretical deficiencies due to the behavior of the Pauli Hamiltonian at the nucleus, which lead to variational collapse for increasing basis set size.³⁰ It was shown that the scalar relativistic correction could account for up to 70% of the total energy in the adsorption of carbon monoxide on platinum and the calculated adsorption site was influenced by the use of relativistic corrections.²⁶ The ZORA formalism requires a special basis set, to include much steeper core-like functions, that are implemented in the code. Within this basis set the double- ζ (DZ) basis functions were used for platinum. For second-row elements and hydrogen double- ζ polarized (DZP), triple- ζ plus polarized (TZP), and triple- ζ plus double polarization (TZ2P) basis functions were used.³¹ The local part of the exchange and correlation functional was modeled using a Vosko, Wilk, Nuisar parametrization of the electron gas.³² The nonlocal part of the functional was modeled using the Becke correction for the exchange³³ and the Perdew correction for the correlation.³⁴ All calculations were run unrestricted. Noncorrected adsorption energies were calculated by using the following formula

$$\Delta E_{\text{ads}} = E_{\text{cluster+adsorbate}} - E_{\text{cluster}} - E_{\text{free molecule}}$$

where $E_{\text{cluster+adsorbate}}$ is the energy of the cluster with the adsorbed molecule, E_{cluster} is the energy of the isolated cluster, and $E_{\text{free molecule}}$ is the energy of the free molecule. Corrections were made in two steps: by inclusion of a partial relaxation of the metal cluster (setting free the degrees of freedom of the central seven atoms of the cluster),^{9,10} which resulted in an increased adsorption energy, and by inclusion of the basis set superposition error (BSSE) using the counterpoise correction according to Boys and Bernardi,³⁴ which decreased the value of adsorption energy. For rigid clusters (where no partial relaxation was applied) and for the rigid part of the partially relaxed clusters the bond distances for platinum were fixed to the experimental value of 2.775 Å for bulk metal.³⁵ Molden³⁶ was used as the graphical interface.

Catalytic Hydrogenations. The 5 wt % Pt/Al₂O₃ catalyst (Engelhard, E4759) was prereduced before use in a fixed-bed reactor by flushing with N₂ at 400 °C for 30 min, followed by reductive treatment with H₂ for 120 min at the same temperature. After cooling to room temperature the catalyst was immediately transferred to the reactor. Hydrogenation experiments were carried out in a parallel pressure reactor system (Endeavor – Argonaut Technologies) with 10 ± 2 mg catalyst, 2 mmol substrate and 5 mL dichloromethane stirred (500 rpm) for 14 h at room temperature and at the indicated pressures. Products were analyzed by GC-MS with a Hewlett-Packard Mod. HP 6890 Gas-Chromatograph equipped with a WCOT Fused Silica, Chirasil-DEX CB column, int. diameter 0.25 μ m, ext. diameter 0.25 mm. The MS Mass Selective Detector was a Hewlett-Packard Mod. HP 5973.

Results

Theoretical Calculations. In the present study the adsorption of benzene, **1**, **2**, and **3** is calculated using a metal cluster of 31 platinum atoms to simulate the surface. This approach was already used for benzene, and values of adsorption energies close to the experimental ones were found.^{9,10} Here, those calculations have been refined by adding two corrections: (i) a partial

TABLE 1: Calculated Adsorption Energies for Benzene on a Pt 31 Cluster, Compared to the Experimental Value^a

	rigid			relaxed		exptl
	bridge	hollow(0)	hollow(30)	bridge	hollow(0)	
DZP						
E_{ads} non-BSSE-corrected	26.1	18.1	14.0	46.6	36.1	28.0–30.1 ¹² 19.6–20.6
BSSE benzene	9.4	9.3	7.8	9.3	9.2	
BSSE Pt 31	12.0	11.6	10.3	11.6	9.0	
BSSE Total	22.2	20.9	18.1	20.9	18.2	
E_{ads} corrected	4.7	−4.1	−2.8	25.7	17.9	
TZP						
E_{ads} non-BSSE-corrected	20.9	13.3	10.2	42.0	31.6	
BSSE benzene	1.0	1.0	0.9	1.0	1.0	
BSSE Pt 31	14.1	13.6	12.2	11.6	10.9	
BSSE total	15.1	14.6	13.1	12.6	11.9	
E_{ads} corrected	5.8	−1.3	−2.9	29.4	19.7	
TZ2P						
E_{ads} non-BSSE-corrected				41.0	31.1	
BSSE benzene				0.8	0.9	
BSSE Pt 31				11.8	13.9	
BSSE total				12.6	14.8	
E_{ads} corrected				28.4	16.3	

^a When the cluster is partially relaxed, the hollow adsorption mode shifts to the more stable bridge mode. Addition of both BSSE correction and of partial relaxation of the cluster, together with a TZP basis set for benzene, results in a practically exact reproduction of the experimental adsorption energy.

relaxation of the metal cluster, consisting of optimizing the geometry of the seven central atoms of the cluster, thus simulating the response of the surface to the chemisorption of the molecule, and (ii) the calculation of the basis set superposition error (BSSE) with the counterpoise correction.³⁴ Furthermore, the dependence of the energy on the basis set (for second row elements) is tested. Table 1 gives the results of this study for benzene in dependence of the correction applied and of the basis set (DZP, TZP, and TZ2P).

We shall analyze first the results for the basis set DZP. As reported previously, the use of a rigid cluster and no BSSE correction provides a reasonable value for the adsorption energies of the bridge and hollow sites. The energies of the bridge and hollow(0) sites compare well to the experimental values, the discrepancy being an underestimation by 2–3 kcal/mol and 1–2 kcal/mol for the bridge and the hollow(0) site, respectively. Hollow(30) sites are less stable than the hollow(0) sites by ca. 4 kcal/mol with this basis set. When the partial relaxation of the metal cluster is applied, hollow(30) sites relax to bridge sites, while the other sites increase their adsorption energy by almost a factor two. Addition of the BSSE correction lowers the adsorption energy by approximately 20 kcal/mol, therefore giving a contribution almost equal to that due to partial cluster relaxation, but in the opposite direction. Using this basis set the quality of the values of adsorption energies after application of the two corrections together are very close to those obtained by applying no correction, for this reason the adsorption energies are comparable to those obtained with the experimental data.

When the basis set is increased to TZP, the adsorption energies decrease. In this case their values without corrections do not reflect the experimental values, but after application of both corrections they almost perfectly coincide with experiment. A further increase of the basis set to TZ2P decreases the correspondence between theory and experiment.

In conclusion, (i) the partial relaxation of the cluster and BSSE are corrections that tend to cancel each other; (ii) the DZP basis set gives very good agreement to experiment without any correction; (iii) the TZP basis set gives the best correspondence to experiment when both corrections are applied

(but poor agreement when no correction is applied); (iv) both DZP with no correction and TZP with both corrections reflect the relative adsorption energies between bridge and hollow sites.

When using the preceding results to simulate the adsorption of **1**, **2**, and **3** it should be noted that upon adsorption on a bridge site the chemical equivalence of the six carbon atoms of (unbound) benzene is lost. The apical carbon atoms C(1) and C(4) each interact with one single platinum atom, while the nonapical carbon atoms C(2)–C(3) and C(5)–C(6) interact with the metal by sharing one platinum atom as binding site (Figure 1). Also note that apical and nonapical carbons have different rehybridization. For benzene (TZP with corrections), the deviation of the C–H bond from the plane is of 42° for the apical position and of 15° for the nonapical position, close to the values reported already.⁹ The symmetry break is caused by a significant distortion of the adsorbed molecule, and a twofold symmetry is obtained.¹³ On the contrary, benzene adsorbed on hollow(0) sites maintains the equivalence of the C atoms. When the methoxy group is added to bridge adsorbed benzene, two possible situations are generated according to whether the carbon atom involved in the bond with the substituent is apical or nonapical (apical and nonapical substitution). Besides the apical and nonapical positions of substitution, the relative position of the methoxy group to the surface can also generate two further structures where the substituent is either in contact with the metal or is above the surface. Methoxy substitution on hollow(0) adsorbed benzene is equivalent on each carbon atom. Figure 2 shows the four calculated adsorption modes of **1** found on platinum. The methoxy group is found in the apical position in adsorption modes B1 and B2, perpendicular to the surface in B1, and in contact with the metal in B2. In this case the position of methoxy perpendicular to the surface is not stable and during optimization the contact with the surface is reached by rotation around the C–O bond. The adsorption mode H(0) is the corresponding mode to hollow(0) ring adsorption. Table 2 summarizes the adsorption energies of the adsorption modes calculated with a DZP basis set and a rigid cluster. The conclusions that can be drawn from this table are that for **1** and **2** apical and nonapical substitutions are close in energy, with a slight preference (ca. 3 kcal/mol) for the latter, while this

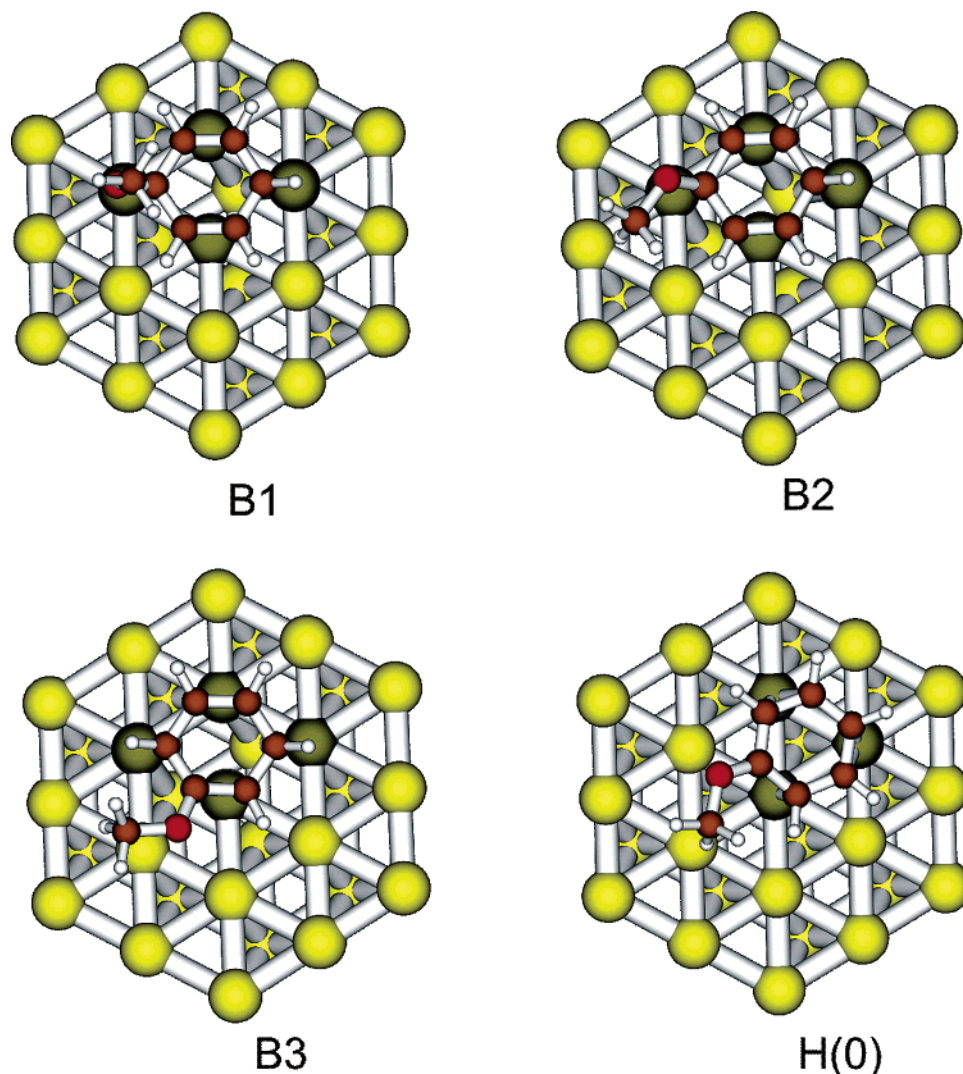


Figure 2. Bridge (B1, B2, and B3) and hollow (H0) adsorption modes of anisole on platinum. B1 and B2 have apical substitution of the methoxy group, whereas B3 has nonapical substitution. In B1 the methoxy substituent is perpendicular to the plane of the metal, whereas in the other conformations it is in contact with the surface.

TABLE 2: Calculated Adsorption Energies of the Bridge and Hollow(0) Sites B1, B2, B3 and H(0) for 1, 2, and 3^a

bridge and hollow(0) adsorption sites: DZP and rigid cluster			
B1	B2	B3	H(0)
anisole			
18.5	22.6	25.7	19.4
3,5-dimethyl-anisole			
16.0	19.9	23.3	16.0
3,5-bis-(trifluorodimethyl)-anisole			
0.0	3.3	15.6	5.4

^a Nonapical substitution and the contact of the OCH₃ group with the metal (B4, Figures 2–4) is the most populated adsorption mode for the three compounds.

difference becomes more pronounced for compound **3**, and furthermore that the methoxy group contributes to the adsorption energy of the molecule on platinum. For adsorption mode B3, the calculation was also performed using a TZP basis set with the addition of the two corrections, cluster relaxation and BSSE (Table 3). The obtained adsorption energy of 25 kcal/mol indicates that anisole is less strongly adsorbed than the parent compound benzene.

The adsorption of **2** was also studied (Table 2 and Figure 3) and analogous to **1**, the B3 adsorption site was found to be the

TABLE 3: Inclusion of Cluster Relaxation and BSSE Correction for the Adsorption Energy of 1, 2, and 3 on Site B3, Using a TZP Basis Set for the Adsorbate

adsorption site B3: TZP basis set, cluster relaxation and BSSE correction				
E_{ads} noncorrected	BSSE adsorbate	BSSE Pt31	BSSE total	E_{ads} corrected
anisole				
41.3	1.2	15.1	16.3	25.0
3,5-dimethyl-anisole				
38.2	1.4	15.6	17.0	21.2
3,5-bis-(trifluoromethyl)-anisole				
26.4	1.9	15.2	17.1	9.3

most stable. The energy of this site decreases by ca. 2 kcal/mol with the DZP basis set, and by ca. 4 kcal/mol with the TZP basis set and addition of corrections (Table 3). The same trend of a decrease of adsorption energy can also be observed for the hollow(0) adsorption site H(0). At first glance it may appear surprising that the loss of adsorption energy is so small relative to **1** considering the steric hindrance of the two methyl groups of this molecule. Two factors have to be considered: (i) the rehybridization of the aromatic carbons, increasing the distance between the methyl group and the surface, alleviating distortions due to repulsion, and (ii) the binding of the methyl groups to

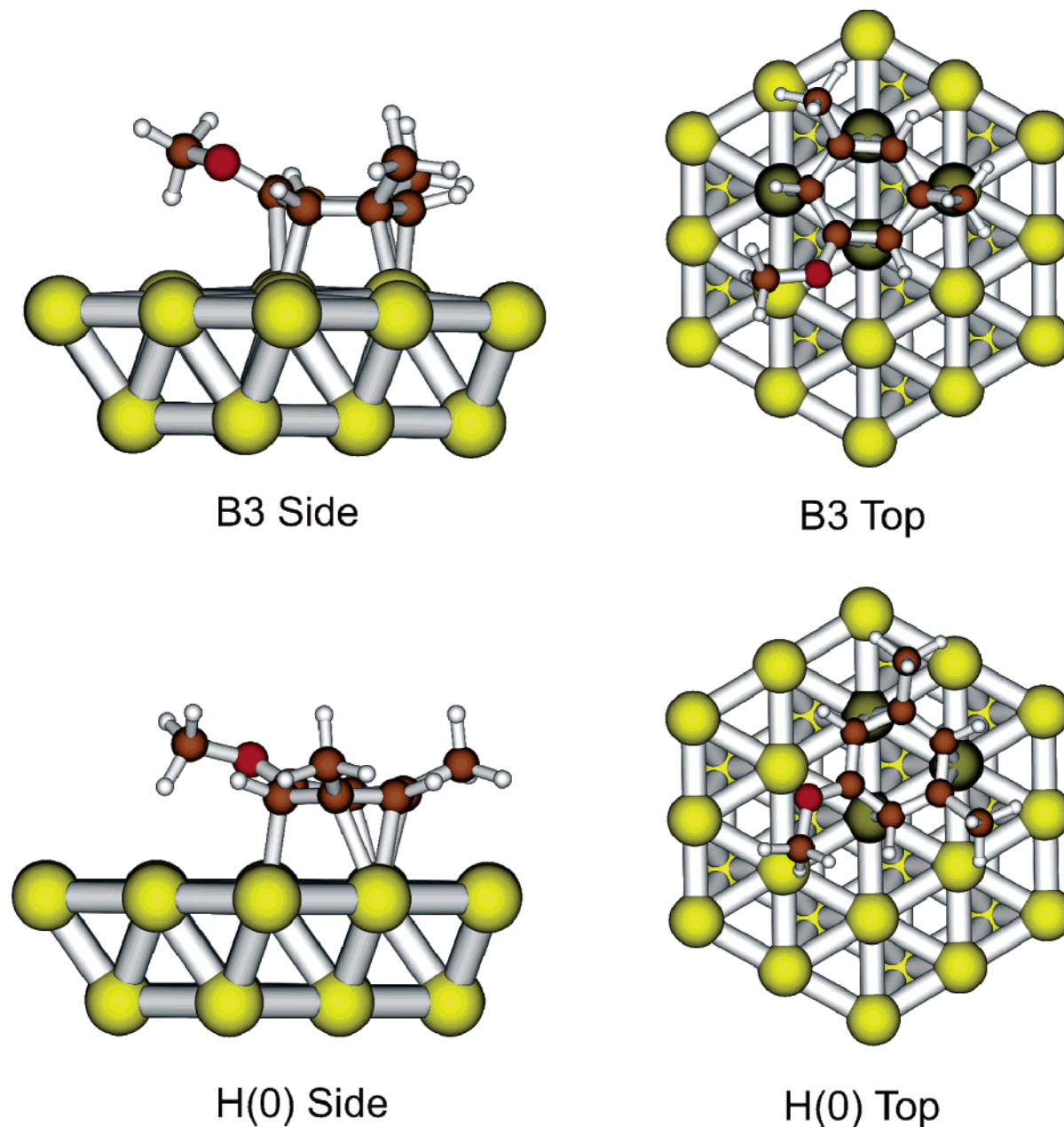


Figure 3. Top and side views of the adsorption modes B3 and H(0) for 3,5-dimethylanisole.

platinum. With respect to the latter point, it has been observed (Table 2) that when a methyl group is in contact with platinum the adsorption energy increases by ca. 3 kcal/mol (see difference between adsorption modes B1 and B2). Although separation of the contribution is not trivial, the methyl groups of **2** partially compensate for repulsion with some binding to the metal.

Compound **3** (Figure 4) was found to behave rather differently. It results from the data shown in Tables 2 and 3 that the adsorption energy decreases substantially for all adsorption sites. In particular for the most stable adsorption site B3, the adsorption energy is less than half that of **2** (with TZP basis set and corrections, Table 3) with a loss of 11.9 kcal/mol. Compared to **1** at the same level of theory, the adsorption energy results lowered by almost 16 kcal/mol. Also note that both bridge and hollow(0) adsorption mode slip to other geometrical arrangements (Figure 4) close to the original but having a different symmetry of the ring skeleton on the site.

To gain insight into the adsorption behavior of the investigated molecules, we analyzed the variations of charge distribu-

tion of metal and adsorbate. The calculated charges (according to the Voronoi deformation density, VDD, scheme)³⁷ for the nonadsorbed substrates, the adsorbed substrates, and platinum are listed in Table 4. In particular, the charges on the aromatic skeleton of the free molecules indicate the effect of the substituents on the electron density on the ring, the charges on the aromatic skeleton for the adsorbed substrates indicate the charge density donated to empty orbitals of the metal by the aromatic ring, and the total charges on platinum indicate the electron density accepted by the metal from the adsorbed molecule. On the free molecules, substitution with methoxy decreases the charge density of benzene and addition of the 3,5-substituents also decreases the electron charge on the ring, following the same trend as the adsorption energy. Also, when the substrates are adsorbed the charge density on the ring decreases from benzene to **1** and from **1** to **2**. But for adsorbed **3** the situation is different, and the electron density on the ring is almost at the same level as for benzene. What happens is clear when the total charge on the metal is considered: while

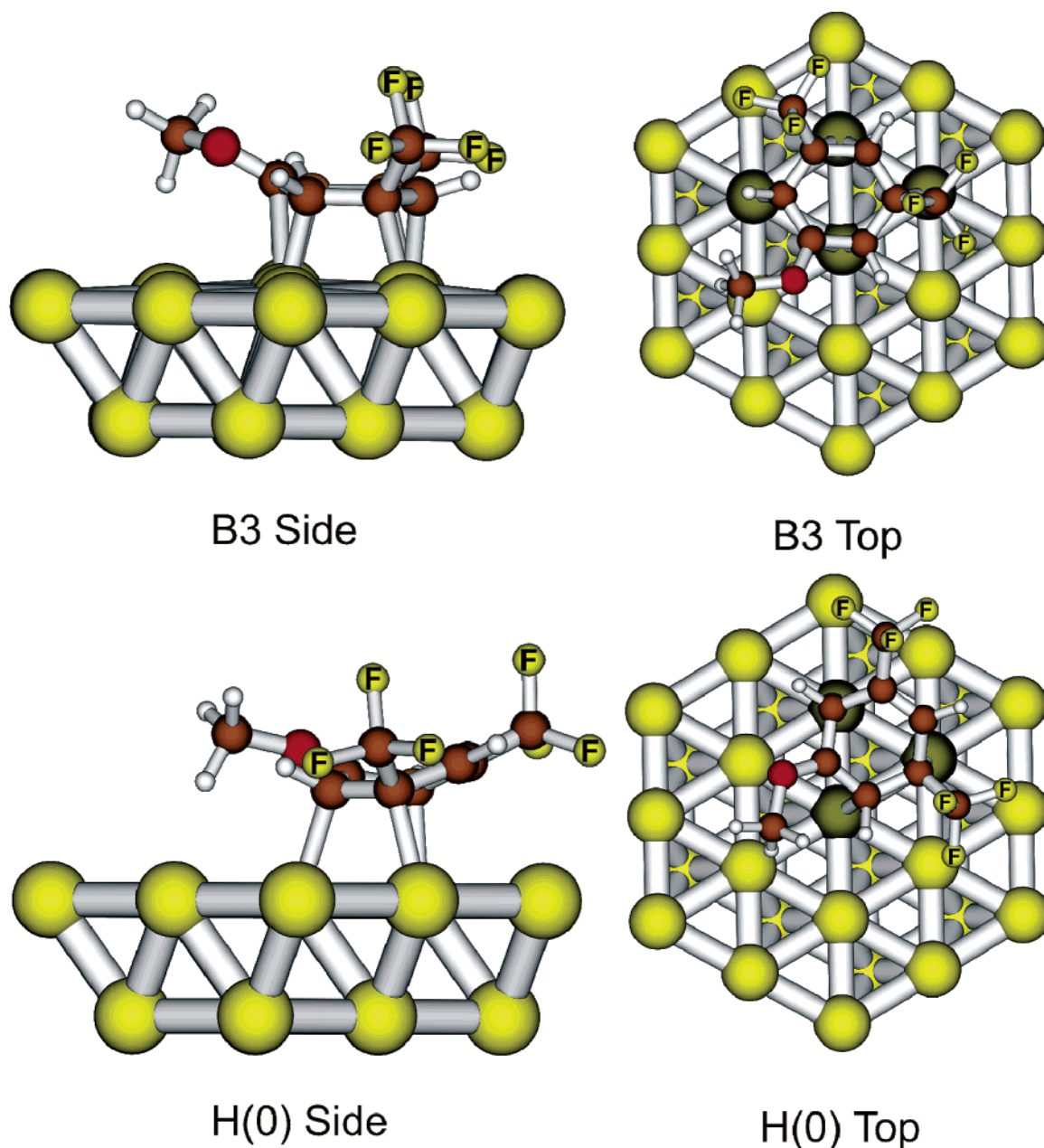


Figure 4. Top and side views of the adsorption modes B3 and H(0) for 3,5-bis-(trifluoromethyl)-anisole.

the charge increases from benzene to **1** and from **1** to **2**, because of the contribution due to the methyl groups close to the metal, in the adsorption of **3** the negative charge on the metal decreases drastically. The trifluoromethyl groups recall electrons from the metal to the aromatic ring, and bonding to the surface results less efficient, in accord with the values found for the adsorption energies.

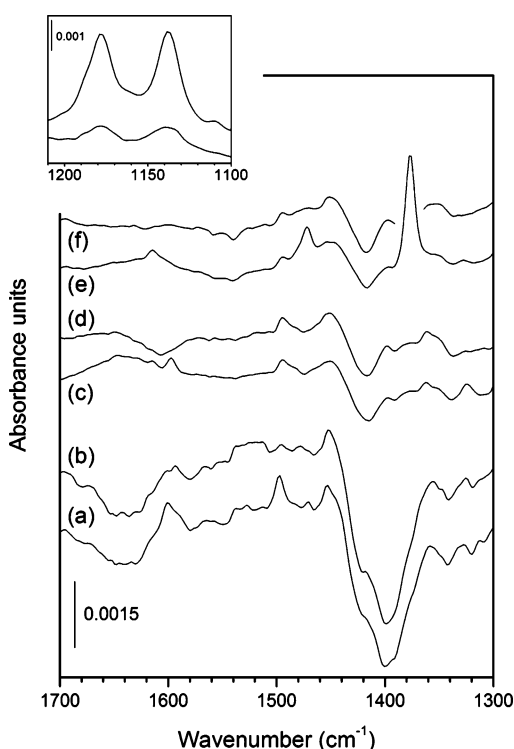
ATR-IR Spectroscopy. Figure 5 displays the ATR-IR spectra obtained when Pt/Al₂O₃ was contacted with a 5 mM solution of **1**, **2**, and **3** in H₂-saturated CH₂Cl₂ solvent. During adsorption, the ATR-IR spectra show signals belonging to all surface species independently from their adsorption strength and only partially to dissolved species. Spectra b, d, and f correspond to the state of the metal surface when rinsing with H₂-saturated CH₂Cl₂ after adsorption of the substituted anisoles and are representative for the most strongly adsorbed species. Spectra a and b are characterized by the broad negative signal at ca. 1400 cm⁻¹, which indicates removal of CH_x-like fragments from the metal surface upon adsorption of the selected compound.²⁴ Analysis

of the ATR-IR spectra is restricted to the 1700–1300 cm⁻¹ spectral region because of the lower signal-to-noise ratio below 1100 cm⁻¹ and because of the lack of significant absorptions. The adsorbates appeared stable against decomposition to CO, which was not observed.

At least two species can be found adsorbed on Pt for the three anisoles, whose adsorption strength is significantly different. The two species differ in the orientation of the benzene ring with respect to Pt and are best identified in the case of **1**.¹⁶ Information on the presence of the two species is provided mainly by the observation that the spectra of **1** on Pt can differ significantly from the neat compound depending on the solute concentration. For low concentrations (<0.5 mM), the presence of only the signals belonging to the deformations of the methyl group indicates that the aromatic ring lies approximately parallel to the surface in one species. At the concentration shown in Figure 5, the spectra display additional bands at 1601 and 1497 cm⁻¹, which suggest a nonparallel adsorption mode for a second species. The resemblance to the spectrum of neat **1** (Supporting

TABLE 4: Charge Transfer between Adsorbate and Metal (According to the Voronoi Deformation Density, VDD, Scheme)^a

charges	
total charges on nonadsorbed benzene skeleton	
benzene	-0.318
anisole	-0.262
3,5-dimethylanisole	-0.226
3,5-bis(trifluoromethyl)anisole	-0.187
total charges on C6 for adsorbed substrates	
benzene	-0.258
anisole	-0.177
3,5-dimethylanisole	-0.147
3,5-bis-(trifluoromethyl)-anisole	-0.254
total charges on platinum	
benzene	-0.174
anisole	-0.252
3,5-dimethylanisole	-0.284
3,5-bis-(trifluoromethyl)-anisole	-0.070

^a Adsorption mode B3, TZP basis set with cluster relaxation.**Figure 5.** In situ ATR-IR spectra of (a) anisole, (c) 3,5-dimethylanisole, (e) 3,5-bis-(trifluoromethyl)-anisole on Pt/Al₂O₃ during adsorption from H₂-saturated CH₂Cl₂ solutions. Spectra have been recorded after 45 min on stream. Spectra b, d, and f were collected when rinsing with H₂-saturated CH₂Cl₂. Conditions: 5 mM in CH₂Cl₂, temp: 20 °C. Inset: ATR-IR spectra of 3,5-bis-(trifluoromethyl)anisole at a solution concentrated of 5 mM (top) and 0.5 mM (bottom).

Information) suggests that interaction of the second species with the metal surface does not perturb the electron distribution of the C₆ ring. Upon rinsing with CH₂Cl₂ solvent the ring deformation modes are strongly attenuated, whereas the signal at 1460 cm⁻¹ remains unperturbed. These changes indicate that the species with the benzene ring nearly parallel to the surface is more stable on Pt than the tilted species. It should be noted that tilted species have not been calculated for **1** and its derivatives because their existence is basically driven by lateral interactions due to surface crowding.

Derivatives **2** and **3** behave similar to **1** with respect to the stability of the two species. The spectrum of **2** on Pt does not

TABLE 5: Assignment of the Vibrational Modes of Neat **2 and Adsorbed on Pt/Al₂O₃ at 20 °C**

calcd ^a	neat ^b	Pt ^c	assignment
1615	1613		$\nu(\text{CC}) + \delta(\text{CH})$
1601	1597	1597	$\nu(\text{CC}) + \delta(\text{CH})$
1483	1467		$\delta_{\text{as}}(\text{CH}_3)_{\text{m}} + \delta_{\text{as}}(\text{CH}_3)_{\text{Ar}} + \delta(\text{CH})$
1478	1467	1495	$\delta_{\text{as}}(\text{CH}_3)_{\text{m}} + \delta_{\text{as}}(\text{CH}_3)_{\text{Ar}} + \delta(\text{CH})$
1471	1467		$\delta_{\text{as}}(\text{CH}_3)_{\text{m}} + \delta_{\text{as}}(\text{CH}_3)_{\text{Ar}}$
1457	1441	1450	$\delta_{\text{as}}(\text{CH}_3)_{\text{m}}$
1453	1441		$\delta_{\text{as}}(\text{CH}_3)$
1449	1441		$\delta_{\text{as}}(\text{CH}_3)_{\text{Ar}} + \delta_{\text{s}}(\text{CH}_3)$
1422	1376		$\delta_{\text{as}}(\text{CH}_3)_{\text{Ar}} + \nu_{\text{s}}(\text{CH}_3)$
1342	1323		$\nu(\text{CC}) + \nu(\text{CH}_3)_{\text{Ar}} + \delta(\text{CH})$
1290	1295		$\nu(\text{CH}_3)_{\text{Ar}} + \delta(\text{CH})$
1188	1193		$\nu(\text{CH}_3)_{\text{Ar}} + \delta(\text{CH})$
1163	1167		$\nu(\text{CH}_3)_{\text{Ar}} + \delta(\text{CH})$
1149	1151		$\nu(\text{CH}_3)_{\text{Ar}} + \delta(\text{CH})$
1073	1072		$\nu(\text{CH}_3)_{\text{m}} + \delta(\text{CH})$

^a B3LYP 6-31Gd,p; frequencies have been scaled by a factor 0.97.^b Transmission mode, CaF₂ windows, ambient temperature. ^c Pt/Al₂O₃, 20 °C, H₂-saturated CH₂Cl₂. Subscript m = methyl group of -OCH₃, Ar = benzene ring.

show significant additional bands to that of **1**. Signals are observed at 1597, 1495, and 1460 cm⁻¹, the former (ring mode, Table 5) disappearing with solvent rinsing. Vibrational analysis indicates that the two remaining features belong to the methyl substituents and the methoxy group, respectively.

Additional strong signals appear at 1377, 1179, and 1138 cm⁻¹ (Figure 5e) in the case of the adsorption of **3** on Pt, which make compound **3** an interesting exception because the ATR-IR spectrum can be extended to the lower frequency region. The two latter signals are also observed at lower concentration (0.5 mM, bottom spectrum of the inset). The signal at 1377 cm⁻¹ includes the symmetric C-CF₃ stretch and symmetric (umbrella-like) C-F stretch. The signals at 1179 and 1138 cm⁻¹ are associated mainly with the asymmetric C-F stretch and appear as broad strong signals at 1174 and 1132 cm⁻¹ in neat **3** due to the envelope of other modes. In the neat compound the intensity of the low-frequency signal is higher than that at high frequency, whereas in the presence of the metal surface the signal intensity is similar (see inset). This observation suggests that the CF₃ groups probably exhibit a specific orientation with respect to Pt. Similar to **2**, the signals at 1614, 1495, 1472, and 1460 cm⁻¹ belong to the benzene ring, the CF₃ substituents, and the methoxy group (Table 6).

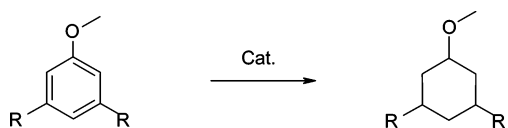
All signals vanish almost completely on solvent rinsing. Only the feature at 1460 cm⁻¹ remains. The disappearance of the signals below 1200 cm⁻¹ for **3** and the fact that they show different ratio with respect to solution (inset of Figure 5) suggest that **3** is predominantly physisorbed in the spectrum in Figure 5e. Because CF₃ groups are usually far stronger infrared absorbers than CH₃ groups, and assuming that if adsorption to the metal in a nearly parallel orientation occurs in both **2** and **3**, the observation of signals due to the methyl groups at 1495 cm⁻¹ (Figure 5d) and that those corresponding to the CF₃ groups disappear during desorption (Figure 5f) might suggest an order of adsorption strength for the two derivatives of **1**. Hence, a higher surface concentration of **2** is found on Pt after desorption compared to **3**, which might correspond to species showing nearly parallel orientation similar to that shown in Figures 3 and 4. Figure 5 also clearly demonstrates how tilted species of both **2** and **3** are less strongly adsorbed than the corresponding species positioning the benzene ring parallel to Pt, similar to **1**.

Catalytic Hydrogenation on Pt/Al₂O₃. Equivalent samples of **1**, **2**, and **3** were hydrogenated on a commercial Pt/Al₂O₃ catalyst at 5 and 20 bar hydrogen for 14 h at room temperature.

TABLE 6: Assignment of the Vibrational Modes of Neat 3 and Adsorbed on Pt/Al₂O₃ at 20 °C

calcd ^a	neat ^b	Pt ^c	assignment
1620	1630		$\nu(\text{CC}) + \delta(\text{CH})$
1610	1614	1614	$\nu(\text{CC}) + \delta(\text{CH})$
1475	1472	1472	$\delta_{\text{as}}(\text{CH}_3)$
1466	1465	1495	$\delta_{\text{s}}(\text{CH}_3) + \nu(\text{C}-\text{C}) + \delta(\text{C}-\text{H})$
1459		1495	$\delta_{\text{as}}(\text{CH}_3)$
1457		1495	$\nu(\text{C}-\text{C}) + \delta_{\text{s}}(\text{CH}_3) + \delta(\text{C}-\text{H})$
1438	1465	1450	$\delta_{\text{s}}(\text{CH}_3) + \delta(\text{C}-\text{H})$
1363	1378	1377	$\nu_{\text{s}}(\text{C}-\text{CF}_3) + \delta(\text{CH}_3) + \nu(\text{C}-\text{O}) + \delta(\text{C}-\text{H})$
1330	1326		$\nu_{\text{as}}(\text{C}-\text{CF}_3) + \delta(\text{CH}_3) + \delta(\text{C}-\text{H})$
1259			$\delta(\text{C}-\text{H})$
1253	1281		$\nu_{\text{s}}(\text{C}-\text{CF}_3) + \delta(\text{C}-\text{H}) + \nu(\text{C}-\text{O})$
1232	1238		$\nu_{\text{s}}(\text{C}-\text{CF}_3) + \delta(\text{C}-\text{H})$
1183	1174	1179	$\nu_{\text{as}}(\text{C}-\text{F}) + \delta(\text{C}-\text{H}) + \delta_{\text{s}}(\text{CH}_3)$
1177			$\nu_{\text{as}}(\text{C}-\text{F}) + \delta_{\text{s}}(\text{CH}_3)$
1173			$\delta_{\text{s}}(\text{CH}_3)$
1156	1132	1138	$\nu_{\text{as}}(\text{C}-\text{F})$
1049	1047		$\nu(\text{CH}_3) + \delta(\text{C}-\text{H})$

^a B3LYP 6-31Gd,p; frequencies have been scaled by a factor 0.97.^b Transmission mode, CaF₂ windows, ambient temperature. ^c Pt/Al₂O₃, 20 °C, H₂-saturated CH₂Cl₂.**TABLE 7: Conversion (%) during Catalytic Hydrogenation of Anisole and Its Derivatives^a**

			
R	pressure		
	5 bar	20 bar	
H	100	100	
CH ₃	75	45	
CF ₃	0	0	

^a Conditions: 5 wt % Pt/Al₂O₃, CH₂Cl₂, ambient temperature, 14 h, conc = 0.4 M. See the Experimental Section for details.

The reaction products were analyzed by GC/MS (Table 7). In agreement with what was observed recently,¹⁶ the aromatic ring of **1** was hydrogenated easily under these conditions and the main product was the cyclohexylmethyl ether. Compound **2** was hydrogenated to the corresponding cyclohexyl derivative with a conversion of only 45% at high pressure (20 bar), whereas 75% of conversion was achieved during the same time of reaction at lower pressure (5 bar). Hydrogenation of **3** did not occur under the conditions used in the present experiments.

Discussion

Large metal clusters have been used for the calculation of the adsorption modes and energies of increasingly large molecules, from hydrogen and ethylene⁹ up to the alkaloid cinchonidine.^{10,18} A calculation of the adsorption energy of a molecule on a metal cluster is typically performed on a rigid cluster, which introduces an error due to the neglected response of the surface to adsorption. The choice of the basis set also introduces an uncertainty because the calculated adsorption energy decreases with increasing basis set size,^{9,38} and increasing the quality of the basis set deteriorates the agreement between calculated and experimental values. A further source of error is the basis set superposition error (BSSE). Some values of BSSE have been reported already for benzene adsorbed on a small Pt 3 cluster⁹ and it was concluded that relative energies of adsorption on different sites are affected by this correction less than absolute values. The decrease of BSSE for increasing basis

set quality was almost equal to the decrease in adsorption energy due to the same increase in basis set quality.⁹ Another study on Pt 19 clusters showed that BSSE tends to cancel for energy differences.³⁸ In conclusion, although the relative adsorption energies could be estimated with good confidence without introducing corrections to the rigid cluster calculation, an uncertainty remained concerning the optimal computational procedure to be used to obtain reliable absolute values using metal clusters. In this work by using a Pt 31 cluster and accounting for the two corrections aforementioned and for the effect of the basis set quality it could be shown that BSSE and cluster relaxation tend to cancel, and optimally do so for the TZP basis set. If no correction is applied, thus remarkably reducing the computational time, a smaller basis set better reflects the experimental values. A Pt 31 cluster can accommodate a large range of medium-size molecules, which makes this study interesting for the evaluation of adsorption energies at relatively low computational cost. Comparison between model calculations performed on a Pt(111) surface and experiments performed on a polycrystalline film, as that used for the ATR-IR studies, seems to be a suitable approach because of the low abundance of defects generally encountered on such model systems.²⁴ The Pt(111) surface, being the most stable among the thermodynamically favored faces, has been used vastly as a model for catalytic studies even under conditions far from ideal vacuum.^{9,39,40} Our study provides further evidence for the validity of this approach.

The theoretical study of the adsorption of **1** and of its derivatives **2** and **3** reveals that **3** is clearly less strongly adsorbed on platinum than **1** and benzene and that **2** has more adsorption similarity with **1**. The analysis of the spectra obtained by the adsorption of the anisole derivatives on Pt allows us to set a scale of adsorption strength also based on spectroscopic evidences. The amplitude of the negative signal at 1400 cm⁻¹ is a preliminary indication of the amount of substrates adsorbed.⁴¹ Thus, it appears from Figure 5 that compounds **2** and **3** adsorb less strongly than **1**. Although both nearly parallel and tilted species can be observed at the relatively high concentration used in this study, only the former should be relevant for the following discussion. Figure 5 indicates that **3** has less affinity toward adsorption, as revealed by the disappearance of all signals, including those characteristic of the CF₃ groups (1377, 1179, and 1138 cm⁻¹). The electron withdrawing trifluoromethyl groups recall charge density from the metal to the benzene ring, thus weakening the chemisorption bond, as suggested by the DFT calculations. In contrast, the permanence of the signal at 1495 cm⁻¹ after rinsing with CH₂Cl₂ revealed the presence of strongly adsorbed species of **2**. Hence, a larger difference in adsorption energy is obtained for compound **3** compared to **1**, and the qualitative scale of adsorption strength **1** > **2** > **3** can be drawn from the spectroscopic data.

Furthermore, catalytic experiments showed that saturation of the compounds follows the same trend as the calculated adsorption energies. Derivative **3** does not undergo ring saturation, in line with the very low chemisorption energy calculated for bridge and hollow sites compared to the parent compounds and with the weak adsorption found by ATR-IR spectroscopy. This correlation seems to indicate that a parallel adsorption to the metal is a necessary prerequisite for ring saturation. It has been shown by theoretical calculations that hydrogenation likely occurs on hollow sites where the substrate is less strongly adsorbed.³⁹ Adsorption on hollow sites decreases the transition state energy for hydrogenation of benzene by ca. 5 kcal/mol because of the increase of the energy of the starting surface

configuration. According to the cited study it is likely that the less strongly adsorbed hollow sites are reaction intermediates in the hydrogenation process, while species adsorbed on bridge sites could be spectator species.

In the present study, the adsorption strength of all investigated molecules on hollow sites decreased compared to the bridge sites. Upon ring substitution, the energy of adsorption on hollow sites decreases from **2** to **3**. Assuming similar hydrogenation pathways to benzene,³⁹ the decreased adsorption strength at hollow sites should lead to lower activation barrier. In contrast, Table 7 shows that hydrogenation is hindered from compound **1** to **3**. A possible explanation is that the lowering of the adsorption energies of the reactive intermediates reduces their surface concentration, resulting in a larger decrease of the reaction rate than a possible increase due to destabilization of the surface intermediate. The decrease of adsorption energy is particularly large for **3**. A further feasible explanation is that the distortion of the bridge and hollow sites induced by the substituents leads to a change in the reaction pathway compared to that proposed for benzene.

Evidence in favor of the first proposal is elicited from Table 7, where the increase in hydrogen pressure causes lower conversion in the hydrogenation of **2**. In this case, assuming a Langmuir–Hinshelwood mechanism, the competing adsorption of hydrogen could diminish the surface concentration of the reaction intermediate, showing that this factor is crucial even under conditions apparently favorable for reaction (high pressure).

Conclusions

After identification of the crucial parameters (BSSE, rigid or free-to-relax cluster and basis set) that allow the best simulation of available spectroscopic data on the adsorption of benzene on large Pt clusters, these parameters have been used to investigate the effect of ring substitution on the adsorption energy and adsorption site of the benzene ring. Anisole and its derivatives have been taken into consideration and their adsorption has been simulated using density functional theory (DFT) combined with attenuated total reflection infrared spectroscopy and hydrogenation experiments on a commercial Pt/Al₂O₃ catalyst. The theoretical calculations on a Pt(111) model surface indicate that the substituted anisoles are less strongly adsorbed than benzene in the order anisole > dimethyl- >> di-trifluoro-derivative with a difference in adsorption energy between anisole and the di-trifluoro-derivative of 16 kcal/mol. Insertion of one or more substituents on the benzene ring complicates the population of possible adsorption sites due to the loss of chemical equivalence of the six carbon atoms of the ring. A bridge adsorption site named B3 has been identified as the most stable for anisole and its derivatives, whereas hollow sites are disfavored and relax to bridge sites similarly to benzene. The infrared spectroscopic data obtained upon adsorption of anisole and its derivatives on Pt model catalysts from the liquid (CH₂-Cl₂) phase indicate an identical but qualitative scale of adsorption strength. Hydrogenation experiments revealed that anisole is quantitatively hydrogenated at 5 bar hydrogen, whereas the affinity to ring saturation decreases in the same order as the scale of adsorption strength, thus strongly supporting a mechanism of hydrogenation based on flat adsorbed intermediates.

The results on the effect of the substitution of the benzene ring with methyl and trifluoromethyl groups on the adsorption energy and site are discussed in a general perspective, which should stimulate future investigation of other important substituents.

Acknowledgment. We kindly acknowledge the Swiss Center for Scientific Computing (Manno) for computational resources and the financial support of the Foundation Claude and Giuliana.

Supporting Information Available: Experimental and theoretical spectra of **1**, **2**, and **3**; Cartesian coordinates of selected structures of Figures 1–4. This material is available free of charge via the Internet at <http://pubs.acs.org>.

References and Notes

- (1) Haq, S.; King, D. A. *J. Phys. Chem.* **1996**, *100*, 16957.
- (2) Abon, M.; Bertolini, J. C.; Billy, J.; Massardier, J.; Tardy, B. *Surf. Sci.* **1985**, *162*, 395.
- (3) Lehwald, S.; Ibach, H.; Demuth, J. E. *Surf. Sci.* **1978**, *78*, 577.
- (4) Somers, J. S.; Bridge, M. E.; Lloyd, D. R. *Spectrochim. Acta, Part A* **1987**, *43*, 1549.
- (5) Horsley, J. A.; Stohr, J.; Hitchcock, A. P.; Newbury, D. C.; Johnson, A. L.; Sette, F. *J. Chem. Phys.* **1985**, *83*, 6099.
- (6) Wander, A.; Held, G.; Hwang, R. Q.; Blackman, G. S.; Xu, M. L.; Deandres, P.; Vanhove, M. A.; Somorjai, G. A. *Surf. Sci.* **1991**, *249*, 21.
- (7) Sautet, P.; Bocquet, M. L. *Isr. J. Chem.* **1996**, *36*, 63.
- (8) Yau, S. L.; Kim, Y. G.; Itaya, K. *J. Am. Chem. Soc.* **1996**, *118*, 7795.
- (9) Saeys, M.; Reyniers, M. F.; Marin, G. B.; Neurock, M. *J. Phys. Chem. B* **2002**, *106*, 7489.
- (10) Vargas, A.; Burgi, T.; Baiker, A. *J. Catal.* **2004**, *226*, 69.
- (11) Hansen, E. W.; Neurock, M. *J. Catal.* **2000**, *196*, 241.
- (12) Xu, C.; Tsai, Y. L.; Koel, B. E. *J. Phys. Chem.* **1994**, *98*, 585.
- (13) Somorjai, G. John Wiley & Sons: New York, 1994.
- (14) Huang, S. X.; Fischer, D. A.; Gland, J. L. *J. Vac. Sci. Technol., A* **1994**, *12*, 2164.
- (15) Cabibil, H.; Ihm, H.; White, J. M. *Surf. Sci.* **2000**, *447*, 91.
- (16) Bonalumi, N.; Vargas, A.; Ferri, D.; Burgi, T.; Mallat, T.; Baiker, A. *J. Am. Chem. Soc.* **2005**, *127*, 8467.
- (17) Baiker, A. *Catal. Today* **2005**, *100*, 159.
- (18) Vargas, A.; Ferri, D.; Baiker, A. *J. Catal.* **2005**, *236*, 1.
- (19) Baiker, A. *J. Mol. Catal. A* **1997**, *115*, 473.
- (20) Ferri, D.; Burgi, T. *J. Am. Chem. Soc.* **2001**, *123*, 12074.
- (21) Vargas, A.; Baiker, A. *J. Catal.* **2006**, *239*, 220.
- (22) Hirschmugl, C. J. *Surf. Sci.* **2002**, *500*, 577.
- (23) Harrick, N. J. *Internal Reflection Spectroscopy*; Interscience Publishers: New York, 1967.
- (24) Ferri, D.; Burgi, T.; Baiker, A. *J. Phys. Chem. B* **2001**, *105*, 3187.
- (25) Baerends, E. J.; Autschbach, J.; Berces, A.; Bo, C.; Boerrigter, P. M.; Cavallo, L.; Chong, D. P.; Deng, L.; Dickson, R. M.; Ellis, D. E.; Fan, L.; Fischer, T. H.; Guerra, C. F.; van Gisbergen, S. J. A.; Groeneveld, J. A.; Gritsenko, O. V.; Gröning, M.; Harris, F. E.; van den Hoek, P.; Jacobsen, H.; van Kessel, G.; Kootstra, F.; van Lenthe, E.; Osinga, V. P.; Patchkovskii, S.; Philipsen, P. H. T.; Post, D.; Pye, C. C.; Ravenek, W.; Ros, P.; Schipper, P. R. T.; Schreckenbach, G.; Snijders, J. G.; Sola, M.; Swart, M.; Swerhone, D.; teVelde, G.; Vernooijs, P.; Versluis, L.; Visser, O.; van Wezenbeek, E.; Wiesenekker, G.; Wolff, S. K.; Woo, T. K.; Ziegler, T. *ADF - Amsterdam Density Functional*, Release 2004-01 ed.; Scientific Computing and Modelling NV, Vrije Universiteit, Theoretical Chemistry: Amsterdam.
- (26) Philipsen, P. H. T.; van Lenthe, E.; Snijders, J. G.; Baerends, E. J. *Phys. Rev. B* **1997**, *56*, 13556.
- (27) Pacchioni, G.; Chung, S. C.; Kruger, S.; Rosch, N. *Surf. Sci.* **1997**, *392*, 173.
- (28) van Lenthe, E.; Ehlers, A.; Baerends, E. J. *J. Chem. Phys.* **1999**, *110*, 8943.
- (29) Snijders, J. G.; Baerends, E. J.; Ros, P. *Mol. Phys.* **1979**, *38*, 1909.
- (30) Velde, G. T.; Bickelhaupt, F. M.; Baerends, E. J.; Guerra, C. F.; van Gisbergen, S. J. A.; Snijders, J. G.; Ziegler, T. *J. Comput. Chem.* **2001**, *22*, 931.
- (31) van Lenthe, E.; Baerends, E. J. *J. Comput. Chem.* **2003**, *24*, 1142.
- (32) Vosko, S. H.; Wilk, L.; Nusair, M. *Can. J. Phys.* **1980**, *58*, 1200.
- (33) Becke, A. D. *Phys. Rev. A* **1988**, *38*, 3098.
- (34) Boys, S. F.; Bernardi, F. *Mol. Phys.* **1970**, *19*, 553.
- (35) Khein, A. *Phys. Rev. B* **1995**, *51*, 16608.
- (36) Schaftenaar, G.; Noordik, J. H. *J. Comput.-Aided Mol. Des.* **2000**, *14*, 123.
- (37) Guerra, C. F.; Handgraaf, J. W.; Baerends, E. J.; Bickelhaupt, F. M. *J. Comput. Chem.* **2004**, *25*, 189.
- (38) Vargas, A.; Burgi, T. B.; Baiker, A. *J. Catal.* **2004**, *222*, 439.
- (39) Saeys, M.; Reyniers, M. F.; Neurock, M.; Marin, G. B. *J. Phys. Chem. B* **2003**, *107*, 3844.
- (40) Morin, C.; Simon, D.; Sautet, P. *J. Phys. Chem. B* **2004**, *108*, 5653.
- (41) Maris, M.; Ferri, D.; Königsmann, L.; Mallat, T.; Baiker, A. *J. Catal.* **2006**, *237*, 230.